ISEV

Characterization of protein complexes in extracellular vesicles by intact extracellular vesicle crosslinking mass spectrometry (iEVXL)

Julia Bauzá-Martinez[1,2] | Gad Armony[1,2] | Matti F. Pronker[1,2] | Wei Wu[1,2,3]

[1]Biomolecular Mass Spectrometry and Proteomics, Bijvoet Center for Biomolecular Research and Utrecht Institute for Pharmaceutical Sciences, Utrecht University, Utrecht, The Netherlands

[2]Singapore Immunology Network (SIgN), Agency for Science, Technology and Research (A*STAR), Singapore, Singapore

[3]Department of Pharmacy, National University of Singapore, Singapore, Singapore

Correspondence
Wei Wu, Singapore Immunology Network (SIgN), Agency for Science, Technology and Research (A*STAR), Singapore, Singapore
Email: wu_wei@immunol.a-star.edu.sg

Abstract

Extracellular vesicles (EVs) are blood-borne messengers that coordinate signalling between different tissues and organs in the body. The specificity of such crosstalk is determined by preferential EV docking to target sites, as mediated through protein-protein interactions. As such, the need to structurally characterize the EV surface precedes further understanding of docking selectivity and recipient-cell uptake mechanisms. Here, we describe an intact extracellular vesicle crosslinking mass spectrometry (iEVXL) method that can be applied for structural characterization of protein complexes in EVs. By using a partially membrane-permeable disuccinimidyl suberate crosslinker, proteins on the EV outer-surface and inside EVs can be immobilized together with their interacting partners. This not only provides covalent stabilization of protein complexes before extraction from the membrane-enclosed environment, but also generates a set of crosslinking distance restraints that can be used for structural modelling and comparative screening of changes in EV protein assemblies. Here we demonstrate iEVXL as a powerful approach to reveal high-resolution information, about protein determinants that govern EV docking and signalling, and as a crucial aid in modelling docking interactions.

1 | INTRODUCTION

Extracellular vesicles (EVs) are small heterogenous vesicles that are secreted by virtually all cells in the body. As important mediators of intercellular communication, EVs can cross biological barriers and have consequently been detected in many biofluids (De La Torre Gomez et al., 2018; Raimondo et al., 2011). Most notably, EVs in patient blood have been very informative as disease diagnostics (Hornung et al., 2020; Hoshino et al., 2020), prognostics and means of treatment stratification (Liu et al., 2021; Tian et al., 2021; Zhou et al., 2021). EVs can carry specific biomolecular cargoes ranging from nucleic acids and lipids to proteins and glycoconjugates (Haraszti et al., 2016; Royo et al., 2019; Thind & Wilson, 2016; Williams et al., 2018). Quite recently, even fully loaded human leukocyte antigen molecules with presented antigen peptides (Bauzá-Martinez et al., 2021; Raposo et al., 1996; Synowsky et al., 2017) have been documented from EVs, further alluding to the immunological influence EVs might have in the body. Due to possible tissue-homing properties (De Jong et al., 2019; Elsharkasy et al., 2020; Herrmann et al., 2021; Vader et al., 2016; Zipkin, 2020), EVs have also been viewed and tested as drug delivery vectors, although the mechanisms governing tissue-specific EV docking still remain poorly understood.

Through understanding the complex biogenesis of EVs (Raposo & Stoorvogel, 2013), it appears inevitable that EVs would co-package cellular bits from their cells of origin that recapitulate their signalling state (Haraszti et al., 2016). Intriguingly, the uptake of activated proteins packaged in EVs by recipient cells could also transfer and propagate oncogenic signalling in the recipient cells (Zhang et al., 2021), hence bypassing the need for prior ligand activation. Such phenomena hold strong significance and

implications in the treatment of malignant disease and cancer metastasis, but also fundamentally explains another mode of inter-cellular crosstalk.

The protein repertoire packaged in EVs and on the surface of EVs is a major determinant of their transit to target sites and function upon recipient-cell uptake. For instance, EVs harbour a large proportion of membrane proteins which can prime the transfer of information between cells by allowing EVs to dock to a target cell or tissue. Although one-to-one specificity between EV markers and target organs has not been extensively established, EV tissue-homing due to specific membrane proteins has been reported (Joshi & Zuhorn, 2021; O'dea et al., 2020; Park et al., 2019). In addition, EVs are also promising vehicles for therapeutic use since they can be naturally or artificially loaded (Pham et al., 2021) with functional components such as enzymes or nucleic acids (Jafari et al., 2020; Khan et al., 2021). In view of these exciting applications, there remains a crucial knowledge gap in specific EV targeting that should be addressed. For instance, which proteins and protein assemblies can facilitate specific tissue targeting, therapeutic packaging and how these components can connect the distribution of EVs to inherited function in recipient cells.

Advances in mass spectrometry have enabled sensitive characterization of the EV protein repertoire (Jeppesen et al., 2019; Rontogianni et al., 2019; Zhang et al., 2018), thereby expanding our knowledge on EV heterogeneity. Nonetheless, these studies use methods that do not inform on the structural aspects of EV protein cargo, which are critical to mechanistically explain EV docking and uptake (Cvjetkovic et al., 2016). Structural characterization of proteins in EVs requires strategies that can directly retrieve structural information without protein extraction, solubilisation or detachment of proteins and protein complexes from the lipid environment. Ideally, any such procedure should also take into consideration the low sample amount and inherent heterogeneity of EVs. These pre-requisites still pose a great challenge even to state-of-the-art technologies such as super-resolution, atomic-force, and electron microscopy, where only a few proteins can be studied simultaneously (Kim et al., 2019; Lennon et al., 2019; Parisse et al., 2017; Zeev-Ben-Mordehai et al., 2014).

Leveraging on advances in crosslinking mass spectrometry (Chavez et al., 2018; Chen et al., 2019; Gonzalez-Lozano et al., 2020), and our recent breakthrough in extracellular crosslinking of whole-cells (Armony et al., 2021), we present here an intact EV crosslinking mass spectrometry (iEVXL) approach, for the systematic characterization of protein complexes in EVs. Using a pair of metastatic breast cancer cell lines, MDA-MB-231 and the metastatic-derived counterpart LM2 (Minn et al., 2005), we demonstrate here that iEVXL can provide high-resolution and comparative structural information that accurately recapitulates the native structure of previously reported complexes. Furthermore, such structural information in the form of distance restrains can aid in mapping unknown protein structures when adequately combined with computational modelling, and iEVXL can also enable hypothesis-free screening of differential protein-assemblies in EVs. This presents a significant step towards structural characterization of supramolecular complexes present in EVs, and functional elucidation of EV protein complexes responsible for homing and docking mechanisms.

2 | RESULTS

2.1 | EV isolation and characterization

EVs were isolated from MDA-MB-231 and LM2 breast cancer cell lines using an ultracentrifugation protocol (Figure 1a) and the quality of the EV preparations was assessed by multiple biochemical and biophysical techniques, according to the MISEV guidelines (Théry et al., 2018) (Figure 1b-e). We confirmed that our EV preparations are significantly enriched for proteins from exosomes, plasma membrane and focal adhesions using a sensitive shotgun proteomics experiment (Figure 1b). Amongst these, EV markers such as CD9, CD63, CD81, TSG101 and PDCD6IP (Alix), were consistently enriched in EVs from both cell lines (Figure 1c). CD81 enrichment in EV preparations was also validated by Western Blot (Figure S1). As previously reported, HLA proteins were also highly enriched in EVs when compared to cells (Bauzá-Martinez et al., 2021) (Figurs 1C). In addition, the integrity, size distribution and concentration of the EV populations were determined by biophysical methods. Imaging by negative stain transmission electron microscopy (NS-TEM) showed that EVs derived from both MDA-MB-231 and LM2 are largely intact after isolation (Figure 1d). Nanoparticle tracking analysis (NTA) revealed that the EV concentration and size distribution between MDA-MB-231 and LM2 are similar, with a particle:protein ratio (purity) of 2×10^9 and particle size of 110 nm, which are expected for ultracentrifugation preparations (Figure 1e). Collectively, these data indicate high quality and purity of the EVs isolated from both MDA-MB-231 and LM2 cell lines.

2.2 | Intact extracellular vesicle crosslinking (iEVXL)

Structural characterization of protein complexes in EVs presents unique challenges, since the phospholipid-bound entities are different in chemical accessibility and biochemical composition compared to a cell lysate. EVs are naturally densely loaded with membrane proteins which can be hard to solubilize while preserving their structure and interactions. In this work, we studied the EV interactome by iEVXL. Compared to conventional strategies of interactome profiling that require prior solubilisation and
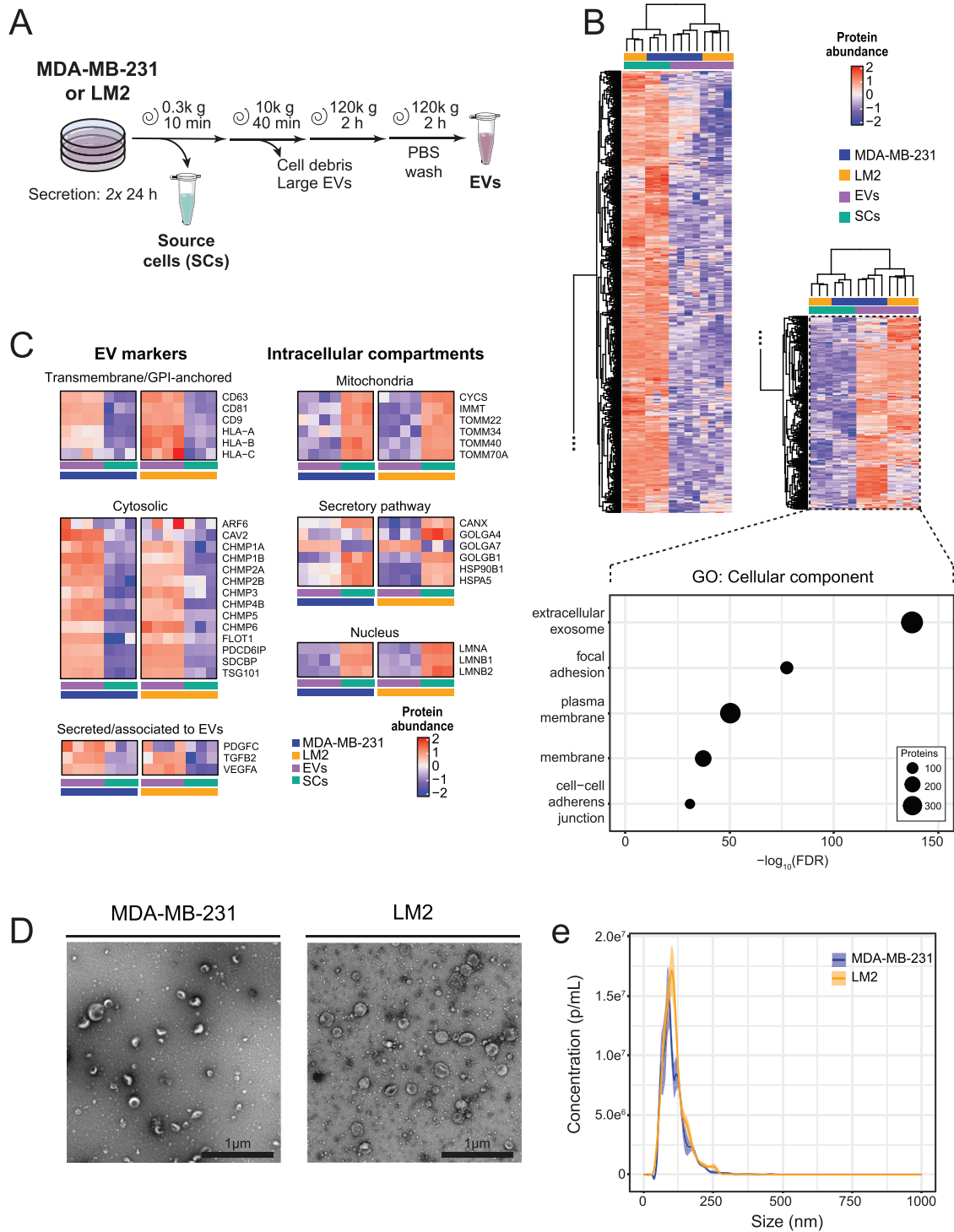
FIGURE 1 **Extracellular vesicle isolation and characterization**. (a) Schematic workflow for EV isolation. MDA-MB-231 or LM2 source cells (SCs, green) or EVs (purple) were harvested by centrifugation and ultracentrifugation, respectively, for further characterization and crosslinking mass spectrometry. (b) Heatmap of proteins significantly enriched in SCs or EVs, based on Student's T-test (q-value < 0.05). EV-enriched proteins were significantly enriched for the GO:CC terms of "extracellular exosome", "plasma membrane" and "focal adhesion" (insert). Dot size represents the number of proteins mapped to each term, and the top five most significantly enriched terms based on false discovery rate (FDR) were plotted. (c) Relative abundance of EV and intracellular compartment marker proteins. EV preparations were significantly enriched with EV markers and depleted of intracellular compartment proteins. (d) Negative stain transmission electron microscopy (NS-TEM) analysis showing the morphology and integrity of the isolated EVs used for crosslinking experiments. Representative images. Scale bar: $1\,\mu$m. (e) Nanoparticle tracking analysis (NTA) showing the size and concentration of isolated EVs used for crosslinking experiments. Purity (particle:protein ratio) of EVs was $\sim 2 \times 10^9$, and mean particle size was similar in EVs derived from either cell line
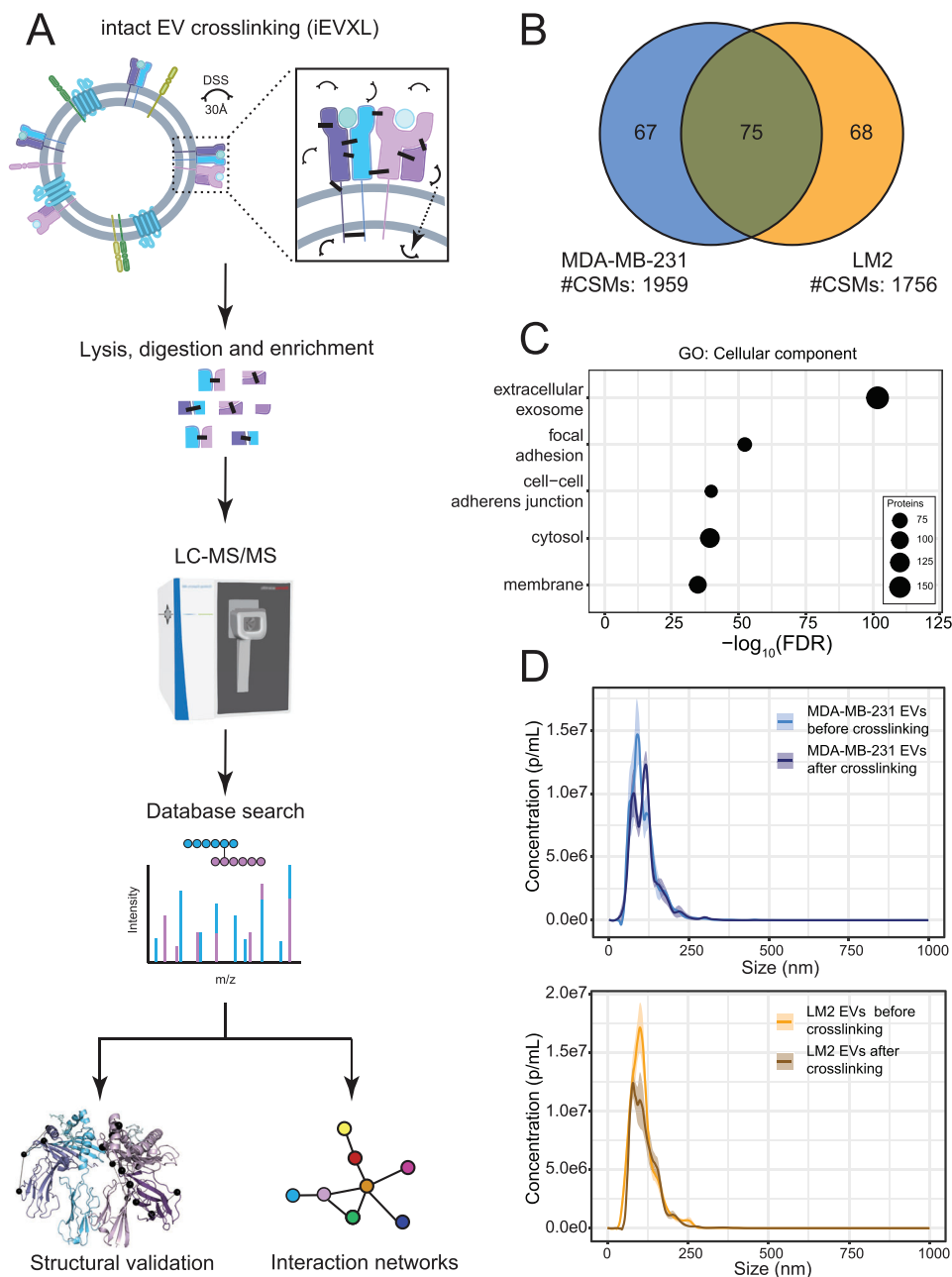
FIGURE 2 **Intact extracellular vesicle crosslinking mass spectrometry (iEVXL).** (a) Schematic workflow used for intact EV crosslinking and LC-MS/MS analysis in the iEVXL pipeline. (b) Overlap between crosslinked proteins in EVs derived from MDA-MB-231 (blue) and LM2 (yellow). The total number of crosslinked peptide spectrum matches (CSMs) is reported for each cell line. (c) GO:CC annotation of crosslinked proteins. Crosslinked proteins were significantly enriched in annotations of "extracellular exosome", "plasma membrane" and "focal adhesion". Dot size represents the number of proteins mapped to each term, and the top five most significantly enriched terms based on false discovery rate (FDR) were plotted. (d) Nanoparticle tracking analysis (NTA). EVs before and after chemical crosslinking were indistinguishable in both size or concentration

extraction of interacting proteins into a non-membranous and aqueous or detergent system (Liu & Heck, 2015; Pankow et al., 2016), crosslinking the EVs directly with a chemical crosslinker allows the preservation of labile protein-protein interactions in their native state before extensive biochemical extraction and purification. Here, we chose to crosslink with disuccinimidyl suberate (DSS), a crosslinker that covalently links lysine residues within a 30Å radius (C_α-C_α distance). The partial membrane permeability of DSS also allows it to penetrate the EV membrane slightly, to access peri-membrane protein complexes on the cytoplasmic side, which may otherwise be missed with membrane-impermeable crosslinkers.

Using a carefully titrated concentration of DSS (2 × 0.5 mM DSS; optimized in Figure S2), we crosslinked EVs derived from a pair of metastatic breast cancer cells lines (Figure 2a). Only after chemical crosslinking, proteins were extracted from the EVs. This would ensure chemical immobilization of interacting proteins in the native orientation before harsh isolation of protein

complexes from their native lipid environment. After DSS crosslinking, denaturing lysis, and trypsin digestion, crosslinked peptides were enriched by strong cation exchange (SCX) chromatography before mass spectrometry analysis of each SCX fraction. The spectral information obtained by LC-MS/MS was then compared with a protein database to retrieve linked peptide pairs (Figure 2a). In the analysis of protein-protein interactions, and structural mapping within protein complexes, we focused largely on the restraints imposed by these crosslinked peptide pairs.

Starting from ∼100 μg of MDA-MB-231 or LM2 EV proteins, we identified 1959 crosslinked peptide spectra matches (CSMs) and 1756 CSMs, respectively. These CSMs originated from about 140 unique proteins in each EV sample, where up to 52% of these proteins were found crosslinked in EVs derived from both cell lines (Figure 2b). Furthermore, crosslinked proteins found in EVs from both cell lines mapped to similar ontology terms (Figure 2c), in strong agreement with the EV proteome (Figure 1b). This provided confidence that crosslinks adequately represent the EV interactome, even with extensive SCX enrichment. Membrane proteins and focal adhesion terms were abundantly mapped in the set of crosslinked proteins (Figure 2c). In addition, the crosslinked positions found within the well-known integral membrane proteins integrin β1, Ep-CAM and CD9 were also consistent with the documented membrane topology, where most of the intralinks were found between residues in the extracellular domain (Figure S3). After crosslinking, size-distribution and concentration of EVs did not change noticeably, as shown by NTA characterization (Figure 2d), indicating that EVs were also not aggregating upon crosslinking. Collectively, these readouts comprehensively ascertain that EVs remain intact and largely free from aggregation at the conditions we used for DSS crosslinking.

2.3 | Structural characterization and modelling of native protein complexes by iEVXL

Experimentally, not only were EVs amenable to our chemical crosslinking workflow (Figure 2), but many crosslinked peptide pairs could also be identified by mass spectrometry subsequently. This provided spectral evidence of EV protein-protein interactions but may also allow structural characterization of native protein complexes in EVs. Coupled to the use of partially membrane permeable DSS as chemical crosslinking agent, we hypothesized it could be possible to retrieve structural information for protein complexes either on the EV external surface, or encapsulated in the EV, but close to the EV membrane. Such data could potentially be very informative to study EV docking, as well as the structural basis of EV interactions with recipient cells. The untargeted nature of iEVXL allows the discovery of important EV protein complexes not known a priori and is also suitable for retrospective interrogation of protein-protein interactions. Most importantly, the unique membrane curvature of EVs could mean that the membrane proteins might have unique intra-membrane conformations which could only be studied with minimally disruptive techniques like iEVXL. We demonstrate this possibility here by mapping the crosslinks found in our dataset on available protein structures, focusing on high abundant EV proteins which have been previously linked to the metastatic potency of EVs.

In this direction, we first examined abundant crosslinks involving α-enolase in this dataset. A-enolase is a glycolytic enzyme commonly found in EVs derived from tumour cells (Almaguel et al., 2020; Didiasova et al., 2019; Jiang et al., 2020), and has been shown to function as a dimer, with its structure previously resolved by X-ray crystallography (Kang et al., 2008). We mapped the α-enolase crosslinks found in our dataset to the high-resolution crystal structure of this protein (PDB: 3b97; 2.2 Å), and all the crosslinks we detected were within the distance of 30 Å, a restraint imposed by the physical length of DSS (Figure 3a). This suggests that XL-MS with DSS on EVs can recapitulate well the natural dimeric structure of α-enolase. Similarly, by mapping the crosslinks involving 14-3-3 proteins detected in the same dataset, we were also able to confirm the validity of crosslinks involving 14-3-3 against the crystal structure of 14-3-3 α/β-heterodimer (PDB: 4dnk, 2.2 Å). In particular, 14-3-3 proteins have been shown to be abundant in oncogenic EVs (Rontogianni et al., 2019; Wang et al., 2018), which is consistent with the metastatic breast cancer origin of our EVs. Since the amino acid resolution of XL-MS could distinguish between the different 14-3-3 isoforms, 'mix-n-match' assembly of 14-3-3 dimers can be distinguished. We mapped all the 14-3-3 crosslinks detected on a representative $\alpha\beta$-heterodimer (Figure 3b). Collectively, these demonstrate proof-of-principle that structural mapping by chemical crosslinking on intact EVs is feasible using a partially membrane-permeable crosslinkers such as DSS, and can detect endogenous protein complexes in documented conformations.

Taking the capabilities of structural mapping one step further, we used structural information from iEVXL to extend partially resolved protein structures. The human moesin protein is highly abundant in MDA-MB-231 and LM2 EVs and contains a poorly characterized long α-helix. To date, a full-length structure of insect (*Spodoptera frugiperda*) moesin has been determined in a closed conformation with its α-helix folded as an antiparallel coiled coil (Li et al., 2007). Small-angle X-ray scattering data combined with crystal structures of the moesin homologue ezrin confirmed this arrangement for human moesin and suggests these proteins can form both inactive monomers and active domain-swapped antiparallel dimers (Phang et al., 2016). From our data, four crosslinks were within the α-helical domain of human moesin, including one between the two supposed α-helices of the coiled coil. Initially, we mapped our data into the AlphaFold (Jumper et al., 2021) predicted human moesin structure, which indeed shows a coiled-coil architecture between residues 350 to 450. Although our crosslinks supported the coiled-coil section of the AlphaFold model, the coiled coil was followed by a long-disordered stretch, decreasing our confidence in the AlphaFold
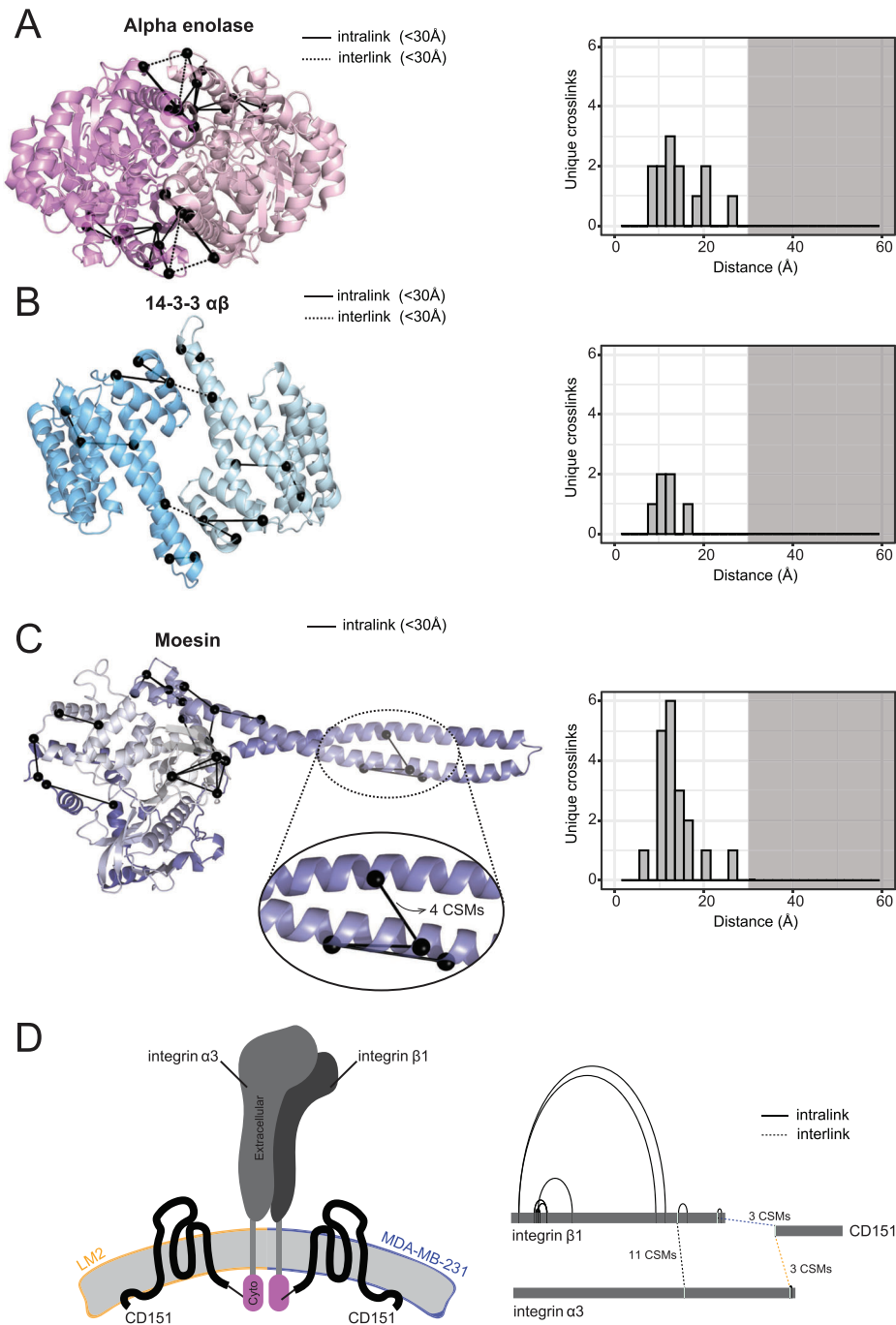
FIGURE 3 **Visualization of detected crosslinks on protein structures**. (a) Crosslinks of EV α-enolase, mapped on high-resolution crystal structure of homodimeric α-enolase (PDB: 3b97). Histogram summarizing the measured Euclidean distances (in Å) between pairs of uniquely crosslinked lysine residues is shown on the right. (b) Crosslinks of EV 14-3-3 mapped on high-resolution crystal structure of 14-3-3 $\alpha\beta$ complex (PDB: 4dnk). (c) Structure of homology-modelled human moesin (coloured in white to blue from N- to C-terminal). Crosslinks mapped on homology-modelled human moesin structure. Insert zooms into residues 375–450 of moesin, a region of the protein that has been proposed to display a coiled-coil type of architecture. Consistent with the length of DSS crosslinker, all crosslinks detected (a-c) were within the Euclidean distances of 30 Å. (d) Mode of interaction for CD151 and integrin α3-β1 dimer in MDA-MB-231 and LM2-derived EVs. Left: proposed mode of interaction via the cytoplasmic tails; Right: protein interaction map showing unique crosslinks detected in EVs that support this interaction model. Blue crosslinks were detected in MDA-MB-231 EVs and yellow crosslinks were detected in LM2 EVs

model. Hence, we instead generated a homology model of human moesin based on the *Spodoptera frugiperda* structure (Li et al., 2007) (PDB: 2I1K). All the crosslinks found in our data were within 30 Å when mapped on the homology-modeled human moesin structure (Figure 3c, histogram). In addition, our crosslinks also supported the coiled-coil type of architecture (Figure 3c, insert) and thus a closed (inactive) conformation of the protein. Therefore, the EV crosslinking data we have generated may also be used

to supplement and weigh-in on contradictory structural reports, to propose the more plausible structure in combination with other structural techniques.

Finally, our iEVXL approach may also allow observations about higher-order structural assemblies, for instance in the interaction between integrin $\alpha_3\beta_1$ dimer and tetraspanin CD151 (Figure 3d). The crosslinks revealed that CD151 interacts with the integrin $\alpha\beta$ dimer via the cytoplasmic tails (Figure 3d, left). Moreover, our data suggested that this interaction can occur in two ways, since the crosslink from CD151 to the α subunit was found exclusively in the LM2 EVs and the crosslink from CD151 to the β subunit exclusively in the MDA-MB-231 EVs (Figure 3d, yellow and blue dotted lines). This interaction has been documented previously by AP-MS (Huttlin et al., 2021) and strongly implicated in metastasis (Brzozowski et al., 2018; Li et al., 2021; Yang et al., 2010; Zhu et al., 2021), although crucial structural information regarding interacting domains could not be inferred from classical interaction studies. This highlights another key advantage of iEVXL as a complementary technique. Therefore, we demonstrate with four examples of structural modelling, that distance restraints from our iEVXL dataset are coherent with complete or partial structures, and that such data can potentially aid in the detailed re-construction of the EV docking interface with recipient cells.

2.4 | Distinct back-to-back annexin A2 conformation in LM2-derived EVs

In the most ideal way, structural profiling should also be sensitive to changes in structural features between closely related systems. To test this, we compared the structural features in EVs derived from MDA-MB-231 and the closely related LM2 cells and found a distinct back-to-back conformation for annexin A2 dimers that was unique to LM2-derived EVs (Figure 4). Annexin A2 is a phospholipid-binding protein involved in the endocytic and exocytic pathways. Annexin A2 is a well-established marker of EVs (Jeppesen et al., 2019), and was abundantly crosslinked in this current dataset. Structurally, annexin A2 has been shown to exist as a monomer, dimer or hetero-tetramer (Roesengarth & Luecke, 2004; Waisman, 1995). Monomeric annexin A2 consists of a concave surface on the bottom and a convex surface at the top, from which it is thought to attach to membranes via protruding lysine and leucine residues (López-Rodríguez et al., 2018) (Figure 4a). Although all the crosslinks found in MDA-MB-231 derived EVs could be explained by monomeric annexin A2 (Figure 4b, blue), five crosslinks found only in LM2-derived EVs exceeded the distance restraints of 30 Å when mapped to the same monomeric annexin A2 structure (Figure 4b, yellow; over-length crosslinks represented by red lines). These distance violations seem to imply that there is substantial non-monomeric annexin A2 in LM2 EVs, but not in MDA-MB-231 derived EVs. Apart from structural differences, protein abundance can sometimes explain fewer crosslinks mapping to a complex. However, Annexin A2 ranked similarly in abundance within each cell line (13th and 16th for LM2 and MDA-MB-231). Hence the non-detection of this back-to-back annexin A2 conformation in MDA-MB-231 is unlikely to be attributed to differential protein abundance alone.

To understand further how the over-length crosslinks that were detected only in LM2-derived EVs might be biologically relevant, we used our crosslinking data for guided molecular modelling. By assuming annexin A2 forms dimers related by C2 rotational symmetry (Plaxco & Gross, 2009), we generated symmetry pairs of intra-protomer crosslinks and analysed the accessible interaction space (Honorato et al., 2021; Van Zundert & Bonvin, 2015; Van Zundert et al., 2017) on annexin A2. Complexes could be found using four out of five pairs of these crosslinks, indicating that these over-length crosslinks were in fact inter-protomer crosslinks. Therefore, we selected these as restraints to guide the subsequent docking process. Out of 200 docked complexes generated by HADDOCK, 186 modelled complexes clustered together, indicating that a single type of interaction is likely to explain the crosslink restraints. From these, we selected the best annexin A2 model based not only on the Haddock scores, but also on complex Matched and Non-accessible Crosslink (cMNXL) scores (Figure S5A, Complex_181w represented by a red dot). While the HADDOCK score is based on Euclidean distances, the cMNXL score is based on the solvent accessible surface distance (SASD). This model revealed a 'back-to-back' conformation, where the convex surfaces from both annexin A2 monomers face the same side (Figure 4c and Figure S5B-C). In further support of this 'back-to-back' annexin A2 conformation, none of the other existing Annexin A2 homodimeric (Roesengarth & Luecke, 2004) (PDB: 1xjl) and heterotetrameric (Ecsédi et al., 2017) (PDB: 5lpu) structures could explain the over-length crosslinks observed specifically in the LM2 dataset (Figure S4).

The inter-protomer interaction surface of annexin A2 was quite large (1172.3 Å^2) and displayed a neutral electrostatic potential as well as quite some hydrophobic patches, indicating a hydrophobicity-based interaction (Figure 4d). Given that residues involved in protein interfaces tend to be more conserved than other residues, we also determined the conservation at the protein surface using all the annexin A2 orthologue sequences present in Uniprot. This analysis revealed that, as expected, the plasma-membrane interacting surface (Figure S6, top view) was highly conserved. The interaction surface found in our 'back-to-back' model was also relatively conserved (Figure S6, back view, interface highlighted in black) when compared to other surfaces, including the lateral surfaces (Figure S6, lateral views 1 and 2) which were previously thought to contribute to annexin A2 oligomerization (Matos et al., 2020). Overall, these results strongly supported a novel 'back-to-back' mode of interaction for annexin A2 in LM2-derived EVs.
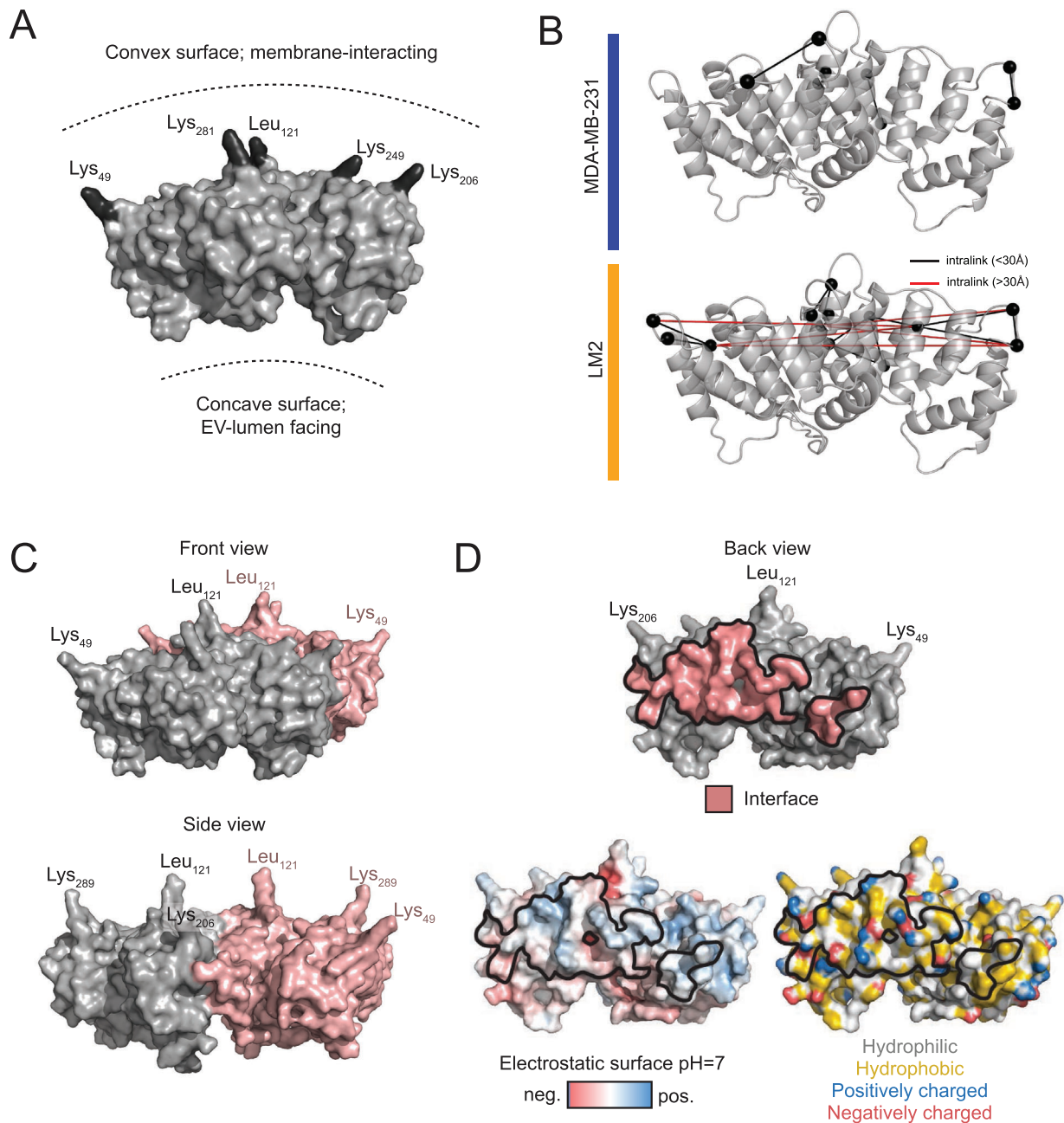
FIGURE 4 **Crosslinking data driven structural modelling for a novel dimeric annexin A2 complex**. (a) Front view of the annexin A2 monomer. Important structural features for annexin A2 functionality are annotated. Residues labelled in the convex surface are involved in plasma membrane interactions. (b) EV crosslinks mapped into the monomeric AlphaFold-predicted structure of annexin A2. Crosslinks detected in MDA-MB-231 (blue) and LM2 (yellow) EVs are plotted separately. (c) Front and side view of annexin A2 crosslinking data driven model. Both copies of annexin A2 interact through the back side, in a back-to-back dimer conformation. (d) Back view of annexin A2 monomer showing the interface (pink), electrostatic surface at pH = 7.0 and hydrophobicity color-coded surface

3 | DISCUSSION

In recent years, EVs have emerged as key mediators of intercellular communication, and have been the focus of many biopharmaceutical and therapeutic developments (Grossen et al., 2021; Herrmann et al., 2021; Zhang et al., 2020; Zipkin, 2020). The protein repertoire and structural features on EVs could critically influence the pharmaceutical utility, as these will ultimately determine tissue-targeting and uptake by recipient cells. In this respect, the advent of sensitive shotgun proteomics has made largescale and detailed EV protein characterization rather feasible, and propelled EVs into the scene of clinical diagnostics (Hoshino et al., 2020; Rontogianni et al., 2019). Nevertheless, the challenge to provide resolution on structural features or topology of EVs

largely remains. Key questions of functional EV targeting require higher resolution mapping of protein complexes and protein conformations in and on the surface of EVs to be further addressed.

Recently, the interest to understand EV structural features (Cvjetkovic et al., 2016) and interactome (Rai et al., 2021) has grown significantly, but techniques amenable to structurally characterize EV protein complexes are remarkably scarce. EVs are unique and heterogenous entities that significantly challenge existing structural methods. Cryo-electron microscopy and tomography are state-of-the-art techniques that have provided a wealth of structural information on many biologically important complexes. Nonetheless, the stringent requirement for sample homogeneity and low complexity complicates the application of such techniques to study EVs. On the other hand, fluorescence-based techniques such as super resolution microscopy still hold a resolution limit of around 20 nm (Galbraith & Galbraith, 2011), which is much larger than the interaction space of a protein complex. In this respect, iEVXL, as we describe here, can bridge with high resolution (< 30Å) structural information on interacting proteins in their native environment. Such data may also complement the information obtained from tomography and fluorescence-based techniques, to collectively sketch the EV docking interface. Therefore, we envision the application of iEVXL as an important step towards understanding EV biology and selective docking mechanisms.

In this technical report, we demonstrate that iEVXL can detect differential protein interactions in EVs, when coupled to chemical crosslinking with partially membrane-permeable crosslinkers such as DSS. We show that detailed and hypothesis-free analyses of EV membrane interactomes are feasible at the scale of ~100 μg of EV proteins, and the structural information obtained are highly reliable and consistent with known experimental structures. With the demonstrated cases of α-enolase, 14-3-3α/β, moesin, CD151- integrin α_3-β_1, and annexin A2 dimers, we showcase a range of utility for iEVXL, in protein structure interface mapping, oligomeric isoform docking, flexible region structural modelling, and determination of higher-order multimeric structural assemblies. As we overcome the generic sensitivity limitations of protein-interaction mass spectrometry, we expect the moderate sensitivity of iEVXL to improve further. Notwithstanding, we envision that the broader application of iEVXL will allow significantly better engineered EV tissue targeting.

4 | METHODS

4.1 | Cell culture and EV isolation

MDA-MB-231 (obtained from ATCC) and LM2 cells (provided by The Netherlands Cancer Institute, NKI) were cultured in DMEM supplemented with 10% fetal bovine serum (FBS; HyClone, USA), 10 mM L-glutamine, 50 U/ml penicillin and 50 μg/ml streptomycin (Lonza) in a humidified incubator at 37°C with 5% CO_2. Cells were detached using 10 mM EDTA/PBS for 5 min at 37°C. Secretion media was prepared by depleting bovine derived EVs from the culture media. To do so, DMEM containing 20% FBS was centrifuged overnight at 100,000 × g at 4°C in a Sorvall T-865 rotor (Thermo Fisher Scientific), filtered on a 0.22 μm Stericup device (Millipore, USA), diluted to 10% FBS, supplemented as previously described and kept at 4°C.

For EV secretion, cells were seeded on 10 plates (15 cm in diameter) at 50% confluence and left to attach overnight. After attachment, cells were gently washed 3× with warm PBS, before addition of secretion media. Conditioned media containing secreted EVs was collected after 24 h and 48 h, fresh secretion media was added to replace the collected conditioned media. Cell viability was measured at the start and end of secretion using the Trypan Blue method, and it remained ~95%. The conditioned media were spun down at 300 × g for 10 min to deplete cells, transferred to clean 50 ml Falcon tubes, spun down at 10,000 × g for 40 min to deplete cell debris and larger vesicles, transferred to clean 50 ml Falcon tubes and kept at 4°C. The two collections were pooled and EVs were immediately pelleted by ultracentrifugation at 120,000 × g, at 4°C for 2 h in a Sorvall T-865 rotor. The pellet was resuspended by gentle pipetting in 10 ml cold PBS supplemented with 50 μg/ml DNAse I (Sigma-Aldrich), to decrease nucleosome contaminations on EV preparations. Purified EVs were finally pelleted again by ultracentrifugation at 120,000 × g at 4°C for 2 h. The EV-pellet was thoroughly resuspended in 400 μl of PBS, spun down at 10,000 × g for 5 min and the EV-containing supernatant was kept. Aliquots were separated for further characterization of the EV populations.

4.2 | EV crosslinking and protein digestion

MDA-MB-231 and LM2-derived EVs were crosslinked using disuccinimidyl suberate (DSS; Thermo Fisher Scientific) with the optimal 0.5 mM crosslinker concentration which was determined in an independent experiment (Figure S1). EV samples (at an average concentration of 7.5 × 10^9 p/ml, 0.5 mg/ml protein in EV lysate) were crosslinked in 0.5 mM DSS for 20 min at RT. To promote crosslinking of lower abundant species, a second round of 0.5 mM DSS was added for another 20 min at RT. The crosslinking reaction was then quenched with 100 mM TRIS pH 8.5 for 5 min. Crosslinked EVs were aliquoted for further characterization. Crosslinked EVs were then lysed by thorough vortexing in 0.5% SDC, 8 M Urea in 50 mM ammonium bicarbonate, followed by 30 min end-to-end rotation at 4°C and 15 cycles of sonication at 4°C (30 s on, 30 s off) in a Bioruptor (Diagenode,

Belgium). Proteins were reduced with 4 mM dithiothreitol (DTT) at RT for 60 min, alkylated with 16 mM iodoacetamide (IAA) at RT for 30 min in the dark which was then quenched by addition of 4 mM DTT. Proteins were first digested by addition of Lys-C (at a 1:50 ratio (w/w); Wako, Japan) at 37°C for 2 h, followed by dilution to 2 M Urea and further digestion with Trypsin (at a ratio 1:50 (w/w); Sigma Aldrich) at 37°C overnight. Protein digestions were stopped by acidification to 5% FA, and precipitated SDC was pelleted by centrifugation at $20,000 \times g$ at 4°C for 30 min. Supernatants were carefully collected, desalted using Sep-Pak C18 cartridges (1cc; Waters, MA, USA), vacuum dried and stored at -20°C until further use.

4.3 | SCX fractionation and enrichment of crosslinked peptides

The desalted peptides were dissolved in 10% formic acid, 2.5% DMSO and loaded on a Luna 100A SCX column (50 mm × 2 mm, 5 μm, Phenomenex product number 00B-4398-B0) with the help of a C18 Opti-Lynx trap column (4.6 mm × 5 mm, 49 μm, Optimize Technologies product number 11-02874-TA). Solvent A consisted of 0.05% formic acid, 20% acetonitrile in water and solvent B consisted of 0.05% formic acid, 20% acetonitrile, and 0.5 M NaCl. The SCX gradient was: 0–10% B in 2 min, 10–40% B in 7 min, 40–80% B in 2.5 min, 80–100% B in 4 min, 100% B for 7 min. One-minute fractions were collected and pooled into six or seven approximately equal fractions by mean UV intensity. The pooled fractions were desalted with Oasis HLA 96-well μElution plate (Waters, MA, USA), vacuum-dried and stored at -80°C.

4.4 | LC-MS/MS of crosslinked SCX fractions

The data was acquired with an Ultimate 3000 system (Thermo Fisher Scientific) coupled to an Orbitrap Exploris 480 mass spectrometer (Thermo Fisher Scientific). Peptides were trapped (Dr. Maisch Reprosil C18, 3 μM, 2 cm × 100 μM) for 2 min in 5% solvent B at a flow rate of 300 nl/min, before being separated on an analytical column (Agilent Poroshell, EC-C18, 2.7 μM, 50 cm x 75 μM). Solvent B consisted of 0.1% formic acid in 80% acetonitrile while solvent A consisted of 0.1% formic acid in water. Crosslinked peptides were then separated in the analytical column at a fixed flow rate of 300 nl/min as follows: each SCX fraction was separated using an optimal 95 min. linear gradient (ranging from 9–40% to 6–35% B) followed by a 3 min steep increase to 99% B, a 5 min wash at 99% B and a 10 min re-equilibration step at 5% A. The mass spectrometer was operated in a data-dependent mode (DDA). Peptides were ionized in a nESI source at 1.9 kV and focused at 40% amplitude of the RF lens. Full scan MS1 spectra from 350 - 2200 m/z were acquired in the Orbitrap at a resolution of 60,000 with the AGC target set to 3×10^6 and under automated calculation of maximum injection time. Cycle time for MS2 fragmentation scans was set to 2 s. Only peptides with charged states 3–8 were fragmented, and dynamic exclusion was set to a duration of 16 ms. Fragmentation was done using a stepped HCD collision energy strategy (NCEs: 28, 31, 34%). Fragment ions were accumulated until a target value of 1×10^5 ions was reached under an automated calculation of maximum injection time, with an isolation window of 1.4 m/z before injection in the Orbitrap for MS2 analysis at a resolution of 30,000. The mass spectrometry proteomics data have been deposited to the ProteomeXchange Consortium via the PRIDE (Vizcaíno et al., 2016) partner repository with the dataset identifier PXD029591.

4.5 | Crosslinking database search and data analysis

For crosslinked peptide analyses, spectra were extracted from "raw" files from precursors ranging between 350 and 20,000 Da, filtered by signal-to-noise ratio of 2 and converted to MGF format using Proteome Discovered software (v2.4, Thermo Scientific). MGF files were searched in pLink 2 (Chen et al., 2019) against a database containing the 1000 most abundant proteins of both MDA-MB-231 and LM2 EV proteomes, as determined in section 4.10., and appended with the sequences of common FBS contaminants to avoid misidentification of crosslinked peptide sequences from *Bos taurus*. The database was further curated to remove signal peptides from the protein sequences (note that positions within proteins still follow the Uniprot numbering). DSS was set as non-cleavable crosslinker and trypsin was set as the digestion enzyme, and up to three missed cleavages were allowed. Peptide length was set to between six and 60 amino-acids, precursor and fragment ion tolerance were set to 10 and 20 ppm, respectively, and oxidation of methionine and acetylation of protein N-terminus were set as variable modifications while carbamidomethylation of cysteines was set as a fixed modification. FDR was set at 1% at all levels, which was calculated by using a reverse decoy database strategy. E-scores were not computed to minimize processing times.

Crosslinking and proteomics data were analysed using Excel and in-house built R scripts (R Development Core Team, R 2011), and plots refined with Illustrator 2020 (Adobe, USA). Spectra and site files from pLink were processed to generate the tables in the supplementary data, and the scripts used to curate pLink outputs have been deposited in GitHub (https://github.com/hecklab/pLink-results-analysis). Only crosslinks identified with sufficient spectral evidence ($\geq$ 2 CSM per cell line) were kept while crosslinks involving histones, a debatable contaminant in EV preparations, were not analysed further. In cases of protein ID ambiguity due to shared crosslinked peptides between different proteins, intra-links were preferred over inter-links.

4.6 | Molecular modelling

A homology model of human moesin (2-577) was generated using Swissmodel (Waterhouse et al., 2018), with the (almost) full-length *Spodoptera frugiperda* moesin structure 2I1K (Li et al., 2007) as a template (homology: 57.89% identity). The N-terminal residue missing from this model was manually added using Coot (Emsley & Cowtan, 2004).

The AlphaFold predicted structure of annexin A2 (Unirpot ID: P07355) was used for the molecular docking procedures. DisVis webserver (Honorato et al., 2021; Van Zundert & Bonvin, 2015; Van Zundert et al., 2017) was used to check compatibility between the crosslinks (including their symmetry mates). Molecular docking was performed with HADDOCK 2.4 web-service (Honorato et al., 2021; Van Zundert et al., 2016). The default parameters of HADDOCK were used with unambiguous restraints based on the crosslinks. The HADDOCK structures were scored based on the crosslinks solvent accessible surface distances (SASDs) using XLM tools (Sinnott et al., 2020). The best docking models were picked based on both the HADDOCK and the cMNXL scores (Bullock et al., 2018). Cocomaps (Vangone et al., 2011) was used to determine which residues were in close contact. The interface was defined as the residues predicted to be in close contact for both annexin A2 copies in the modelled structure. For conservation analysis, all the annexin A2 orthologs present in Uniprot (excluding low quality proteins) were aligned using the Clustal Omega (Sievers et al., 2011) algorithm and the alignment and phylogenetic tree were fed to ConSurf (Ashkenazy et al., 2016) to calculate the conservation score and visualize it on the protein structure.

4.7 | Negative stain electron microscopy (NS-TEM)

Thin layer continuous formvar/carbon-coated copper mesh grids (Ted Pella 400 mesh Cu, 01754-F) were glow discharged for 10 s at 10 mA, and immediately incubated with 3 μl of undiluted EVs in PBS for 45s. Excess solution was blotted away, and the samples were stained first by a quick immersion in 2% (w/v) of uranyl acetate followed by re-staining for 1 min with the same reagent. After each staining step, the excess solution was blotted away. Grids were then dried at RT before electron microscopy imaging. NS-TEM data was collected on a Talos L120C transmission electron microscope (Thermo Fisher Scientific) operated at 120 kV. Images were acquired with a 4k × 4k Ceta CMOS camera (Thermo Fisher Scientific) at a magnification of 11000× corresponding to a pixel size of 13.6 Å.

4.8 | Nanoparticle tracking analysis (NTA)

EVs were analysed in a NanoSight NS500 (Malvern Panalytica, UK), equipped with a sCMOS camera and a Blue405 laser. The camera level was set to 16. The samples were diluted 1:500 in PBS to a final volume of 1 ml to be in the optimal range of operation (between 30–100 particles/frame). Four videos of 1 min were taken at 25 FPS and averaged with the built-in NanoSight Software NTA v.3.4 using a detection threshold of 5.

4.9 | SDS-page and western blot

Lysed EVs or source-cell material were resolved on 12% Bis-Tris Criterion XT precast gels (Biorad, USA) with 1x XT-MOPS buffer at fixed voltage of 150 V for about 2 h. Proteins were stained in-gel using Imperial Protein Stain (Thermo Fisher Scientific). For Western detection, proteins were transferred to a PVDF membrane in Towbin buffer (0.025 M Tris, 0.192 M glycine, 20% methanol) at 100 V and 4°C for 1 h. Membranes were washed 3x with TBS buffer containing 1% Tween-20 (TBST) and then blocked for 1 h in TBST supplemented with 5% Blotting-Grade Blocker (Biorad). Primary antibody (α-CD81 at 1:200) was incubated at 4°C overnight in TBST supplemented with 1% milk. Secondary antibody incubation was done using HRP conjugated α-mouse IgG antibody (1:2000 dilution) for 2 h at RT in the same buffer. Between and after antibody incubations, membranes were washed 3× 10 min in TBST. HRP signal was visualized using SuperSignal West Dura (Thermo Fisher Scientific) substrate, on an Amersham Imager 600 (GE healthcare, USA).

4.10 | MDA-MB-231 and LM2 EV and source cells proteomic characterization

The proteomic characterization of the EVs and source cell proteomes has been done re-using high resolution data previously published (Rontogianni et al., 2019). Cell culture and EV-isolation conditions were the same and the reproducibility of the source cell and EV proteomes was assessed in independent biological replicates for both cells lines under such conditions. Briefly, the "raw" files from four biological replicates of EVs isolated from either MDA-MB-231 or LM2 cells, as well as three biological replicates of their source cells, were downloaded from Proteome Xchange (PXD012162) and re-searched using MaxQuant (v_1.6.5.0) (Tyanova

et al., 2016) against SwissProt human database (downloaded on 09/2019, containing 20,431 protein sequences) appended with common contaminants. Trypsin was set as the digestion enzyme and up to two missed cleavages were allowed. Oxidation of methionine and acetylation of protein N-terminus were set as variable modifications and carbamidomethylation of cysteine was set as a fixed modification. Label-free quantification (LFQ) was enabled using a minimum ratio count of two and both razor and unique peptides for quantification. Match between runs approach was enabled using default parameters. Precursor ion tolerance was set to 20 ppm for the first search and 4.5 ppm after recalibration, and fragment ions tolerance was set to 20 ppm. FDR was set at 1% for both PSM and protein level by using a reverse decoy database strategy.

ACKNOWLEDGEMENTS

AUTHOR CONTRIBUTIONS

Julia Bauzá-Martinez, Gad Armony and Wei Wu conceived this study and designed the experimental approach. JBM performed all cell culture experiments. Julia Bauzá-Martinez and Gad Armony performed all crosslinking experiments and data analysis. Matti F. Pronker performed NS-TEM analysis and assisted with structural modelling and analysis. Julia Bauzá-Martinez and Wei Wu co-wrote this manuscript and Gad Armony, Matti F. Pronker and Wei Wu edited this manuscript.

CONFLICT OF INTERESTS

The authors declare no competing interests.

REFERENCES

Almaguel, F. A., Sanchez, T. W., Ortiz-Hernandez, G. L., & Casiano, C. A. (2020). Alpha-enolase: emerging tumor-associated antigen, cancer biomarker, and oncotherapeutic target. *Frontiers in Genetics*, *11*, 28. PMID: 32117444.

Armony, G., Heck, A. J. R., & Wu, W. (2021). Extracellular crosslinking mass spectrometry reveals HLA class I - HLA class II interactions on the cell surface. *Molecular Immunology*, *136*, 16–25.[CrossRef] PMID: 34052579.

Ashkenazy, H., Abadi, S., Martz, E., Chay, O., Mayrose, I., Pupko, T., & Ben-Tal, N. (2016). ConSurf 2016: An improved methodology to estimate and visualize evolutionary conservation in macromolecules. *Nucleic Acids Research*, *44*, W344–W350.[CrossRef].

Bauzá-Martinez, J., Heck, A. J. R., & Wu, W. (2021). HLA-B and cysteinylated ligands distinguish the antigen presentation landscape of extracellular vesicles. *Communications Biology*, *4*, 825.[CrossRef] PMID: 34211107.

Brzozowski, J. S., Bond, D. R., Jankowski, H., Goldie, B. J., Burchell, R., Naudin, C., Smith, N. D., Scarlett, C. J., Larsen, M. R., Dun, M. D., Skelding, K. A., & Weidenhofer, J. (2018). Extracellular vesicles with altered tetraspanin CD9 and CD151 levels confer increased prostate cell motility and invasion. *Science Reports*, *8*, 8822.[CrossRef] PMID: 29891991.

Bullock, J. M. A., Sen, N., Thalassinos, K., & Topf, M. (2018). Modeling protein complexes using restraints from crosslinking mass spectrometry. *Structure (London, England)*, *26*, 1015–1024.e2.[CrossRef].

Chavez, J. D., Lee, C. F., Caudal, A., Keller, A., Tian, R., & Bruce, J. E. (2018). Chemical crosslinking mass spectrometry analysis of protein conformations and supercomplexes in heart tissue. *Cell Systems*, *6*, 136–141.e5.[CrossRef].

Chen, Z. L., Meng, J. M., Cao, Y., Yin, J. L., Fang, R. Q., Fan, S. B., Liu, C., Zeng, W. F., Ding, Y. H., Tan, D., Wu, L., Zhou, W. J., Chi, H., Sun, R. X., Dong, M. Q., & He, S. M. (2019). A high-speed search engine pLink 2 with systematic evaluation for proteome-scale identification of cross-linked peptides. *Nature Communications*, *10*, 1–12. PMID: 30602773.

Cvjetkovic, A., Jang, S. C., Konečná, B., Höög, J. L., Sihlbom, C., Lässer, C., & Lötvall, J. (2016). Detailed analysis of protein topology of extracellular vesicles-evidence of unconventional membrane protein orientation. *Science Reports*, *6*, 36338.[CrossRef] PMID: 27821849.

De Jong, O. G., Kooijmans, S. A. A., Murphy, D. E., Jiang, L., Evers, M. J. W., Sluijter, J. P. G., Vader, P., & Schiffelers, R. M. (2019). Drug delivery with extracellular vesicles: From imagination to innovation. *Accounts of Chemical Research*, *52*, 1761–1770.[CrossRef] PMID: 31181910.

De La Torre Gomez, C., Goreham, R. V., Bech Serra, J. J., Nann, T., & Kussmann, M. (2018). "Exosomics"-A review of biophysics, biology and biochemistry of exosomes with a focus on human breast milk. *Frontiers in Genetics*, *9*, 92.[CrossRef] PMID: 29636770.

Didiasova, M., Schaefer, L., & Wygrecka, M. (2019). When place matters: Shuttling of enolase-1 across cellular compartments. *Frontiers in Cell and Developmental Biology*, *7*, 61.[CrossRef] PMID: 31106201.

Ecsédi, P., Kiss, B., Gógl, G., Radnai, L., Buday, L., Koprivanacz, K., Liliom, K., Leveles, I., Vértessy, B., Jeszenői, N., Hetényi, C., Schlosser, G., Katona, G., & Nyitray, L. (2017). Regulation of the equilibrium between closed and open conformations of annexin A2 by N-terminal phosphorylation and S100A4-binding. *Structure (London, England)*, *25*, 1195–1207.e5.[CrossRef].

Elsharkasy, O. M., Nordin, J. Z., Hagey, D. W., de Jong, O. G., Schiffelers, R. M., Andaloussi, S. E., & Vader, P. (2020). Extracellular vesicles as drug delivery systems: Why and how? *Advanced Drug Delivery Reviews*, *106*, 148–156.

Emsley, P., & Cowtan, K. (2004). Coot: Model-building tools for molecular graphics. *Acta crystallographica Section D, Biological crystallography*, *60*, 2126–2132.[CrossRef] PMID: 15572765.

Galbraith, C. G., & Galbraith, J. A. (2011). Super-resolution microscopy at a glance. *Journal of Cell Science*, *124*, 1607–1611.[CrossRef] PMID: 21536831.

Gonzalez-Lozano, M. A., Koopmans, F., Sullivan, P. F., Protze, J., Krause, G., Verhage, M., Li, K. W., Liu, F., & Smit, A. B. (2020). Stitching the synapse: Cross-linking mass spectrometry into resolving synaptic protein interactions. *Science Advances*, *6*, eaax5783.[CrossRef] PMID: 32128395.

Grossen, P., Portmann, M., Koller, E., Duschmalé, M., Minz, T., Sewing, S., Pandya, N. J., Van Geijtenbeek, S. K., Ducret, A., Kusznir, E. A., Huber, S., Berrera, M., Lauer, M. E., Ringler, P., Nordbo, B., Jensen, M. L., Sladojevich, F., Jagasia, R., Alex, R., …, Keller, M. (2021). Evaluation of bovine milk extracellular vesicles

for the delivery of locked nucleic acid antisense oligonucleotides. *European Journal of Pharmaceutics and Biopharmaceutics*, *158*, 198–210.[CrossRef] PMID: 33248268.

Haraszti, R. A., Didiot, M. - C., Sapp, E., Leszyk, J., Shaffer, S. A., Rockwell, H. E., Gao, F., Narain, N. R., Difiglia, M., Kiebish, M. A., Aronin, N., & Khvorova, A. (2016). High-resolution proteomic and lipidomic analysis of exosomes and microvesicles from different cell sources. *Journal of Extracellular Vesicles*, *5*, 32570.[CrossRef] PMID: 27863537.

Herrmann, I. K., Wood, M. J. A., & Fuhrmann, G. (2021). Extracellular vesicles as a next-generation drug delivery platform. *Nature Nanotechnology*, *16*, 748–759.[CrossRef] PMID: 34211166.

Honorato, R. V., Koukos, P. I., Jiménez-García, B., Tsaregorodtsev, A., Verlato, M., Giachetti, A., Rosato, A., & Bonvin, A. M. J. J. (2021). Structural biology in the clouds: The WeNMR-EOSC ecosystem. *Frontiers in Molecular Biosciences*, *8*, 729513.[CrossRef] PMID: 34395534.

Hornung, S., Dutta, S., & Bitan, G. (2020). CNS-derived blood exosomes as a promising source of biomarkers: Opportunities and challenges. *Frontiers in Molecular Neuroscience*, *13*, 38.[CrossRef] PMID: 32265650.

Hoshino, A., Kim, H. S., Bojmar, L., Gyan, K. E., Cioffi, M., Hernandez, J., Zambirinis, C. P., Rodrigues, G., Molina, H., Heissel, S., Mark, M. T., Steiner, L., Benito-Martin, A., Lucotti, S., Di Giannatale, A., Offer, K., Nakajima, M., Williams, C., Nogués, L., …, Lyden, D. (2020). Extracellular vesicle and particle biomarkers define multiple human cancers. *Cell*, *182*, 1044–1061.e18.[CrossRef].

Huttlin, E. L., Bruckner, R. J., Navarrete-Perea, J., Cannon, J. R., Baltier, K., Gebreab, F., Gygi, M. P., Thornock, A., Zarraga, G., Tam, S., Szpyt, J., Gassaway, B. M., Panov, A., Parzen, H., Fu, S., Golbazi, A., Maenpaa, E., Stricker, K., Guha Thakurta, S., …, Gygi, S. P. (2021). Dual proteome-scale networks reveal cell-specific remodeling of the human interactome. *Cell*, *184*, 3022–3040.e28.[CrossRef].

Jafari, D., Shajari, S., Jafari, R., Mardi, N., Gomari, H., Ganji, F., Forouzandeh Moghadam, M., & Samadikuchaksaraei, A. (2020). Designer exosomes: A new platform for biotechnology therapeutics. *Biodrugs*, *34*, 567–586.[CrossRef] PMID: 32754790.

Jeppesen, D. K., Fenix, A. M., Franklin, J. L., Higginbotham, J. N., Zhang, Q., Zimmerman, L. J., Liebler, D. C., Ping, J., Liu, Q., Evans, R., Fissell, W. H., Patton, J. G., Rome, L. H., Burnette, D. T., & Coffey, R. J. (2019). Reassessment of exosome composition. *Cell*, *177*, 428–445.e18.[CrossRef].

Jiang, K., Dong, C., Yin, Z., Li, R., Mao, J., Wang, C., Zhang, J., Gao, Z., Liang, R., Wang, Q., & Wang, L. (2020). Exosome-derived ENO1 regulates integrin $\alpha6\beta4$ expression and promotes hepatocellular carcinoma growth and metastasis. *Cell Death & Disease*, *11*, 972.[CrossRef] PMID: 33184263.

Joshi, B. S., & Zuhorn, I. S. (2021). Heparan sulfate proteoglycan-mediated dynamin-dependent transport of neural stem cell exosomes in an in vitro blood-brain barrier model. *European Journal of Neuroscience*, *53*, 706–719.[CrossRef] PMID: 32939863.

Jumper, J., Evans, R., Pritzel, A., Green, T., Figurnov, M., Ronneberger, O., Tunyasuvunakool, K., Bates, R., Žídek, A., Potapenko, A., Bridgland, A., Meyer, C., Kohl, S. A. A., Ballard, A. J., Cowie, A., Romera-Paredes, B., Nikolov, S., Jain, R., Adler, J., …, Hassabis, D. (2021). Highly accurate protein structure prediction with AlphaFold. *Nature*, *596*, 583–589.[CrossRef] PMID: 34265844.

Kang, H. J., Jung, S. - K., Kim, S. J., & Chung, S. J. (2008). Structure of human alpha-enolase (hENO1), a multifunctional glycolytic enzyme. *Acta crystallographica Section D, Biological crystallography*, *64*, 651–657.[CrossRef] PMID: 18560153.

Khan, H., Pan, J. - J., Li, Y., Zhang, Z., & Yang, G. - Y. (2021). Native and bioengineered exosomes for ischemic stroke therapy. *Frontiers in Cell and Developmental Biology*, *9*, 619565.[CrossRef] PMID: 33869170.

Kim, S. Y., Khanal, D., Kalionis, B., & Chrzanowski, W. (2019). High-fidelity probing of the structure and heterogeneity of extracellular vesicles by resonance-enhanced atomic force microscopy infrared spectroscopy. *Nature Protocols*, *14*, 576–593.[CrossRef] PMID: 30651586.

Lennon, K. M., Wakefield, D. L., Maddox, A. L., Brehove, M. S., Willner, A. N., Garcia-Mansfield, K., Meechoovet, B., Reiman, R., Hutchins, E., Miller, M. M., Goel, A., Pirrotte, P., Van Keuren-Jensen, K., & Jovanovic-Talisman, T. (2019). Single molecule characterization of individual extracellular vesicles from pancreatic cancer. *Journal of Extracellular Vesicles*, *8*, 1685634.[CrossRef] PMID: 31741725.

Li, Q., Nance, M. R., Kulikauskas, R., Nyberg, K., Fehon, R., Karplus, P. A, Bretscher, A., & Tesmer, J. J. G. (2007). Self-masking in an intact ERM-merlin protein: an active role for the central alpha-helical domain. *Journal of Molecular Biology*, *365*, 1446–1459.[CrossRef] PMID: 17134719.

Li, S., Li, X., Yang, S., Pi, H., Li, Z., Yao, P., Zhang, Q., Wang, Q., Shen, P., Li, X., & Ji, J. (2021). Proteomic landscape of exosomes reveals the functional contributions of CD151 in triple-negative breast cancer. *Molecular & cellular proteomics*, *20*, 100121.

Liu, F., & Heck, A. Jr (2015). Interrogating the architecture of protein assemblies and protein interaction networks by cross-linking mass spectrometry. *Current Opinion in Structural Biology*, *35*, 100–108.[CrossRef] PMID: 26615471.

Liu, J., Han, Y., Hu, S., Cai, Y., Yang, J., Ren, S., Zhao, Y., Lu, T., Zhou, X., & Wang, X. (2021). Circulating exosomal MiR-107 restrains tumorigenesis in diffuse large B-cell lymphoma by targeting 14-3-3η. *Frontiers in Cell and Developmental Biology*, *9*, 845.

López-Rodríguez, J. C., Martã-Nez-Carmona, F. J., Rodrã-Guez-Crespo, I., Lizarbe, M. A., & Turnay, J. (2018). Molecular dissection of the membrane aggregation mechanisms induced by monomeric annexin A2. *Biochimica et Biophysica Acta*, *1865*, 863–873.[CrossRef] PMID: 29567212.

Matos, A. L. L., Kudruk, S., Moratz, J., Heflik, M., Grill, D., Ravoo, B. J., & Gerke, V. (2020). Membrane binding promotes annexin A2 oligomerization. *Cells*, *9*, 1169.[CrossRef].

Minn, A. J., Gupta, G. P., Siegel, P. M., Bos, P. D., Shu, W., Giri, D. D., Viale, A., Olshen, A. B., Gerald, W. L., & Massagué, J. (2005). Genes that mediate breast cancer metastasis to lung. *Nature*, *436*, 518–524.[CrossRef] PMID: 16049480.

O'dea, K. P., Tan, Y. Y., Shah, S., V Patel, B., C Tatham, K., Wilson, M. R., Soni, S., & Takata, M. (2020). Monocytes mediate homing of circulating microvesicles to the pulmonary vasculature during low-grade systemic inflammation. *Journal of Extracellular Vesicles*, *9*, 1706708.[CrossRef] PMID: 32002170.

Pankow, S., Bamberger, C., Calzolari, D., Bamberger, A., & Yates, J. R. (2016). Deep interactome profiling of membrane proteins by co-interacting protein identification technology. *Nature Protocols*, *11*, 2515–2528.[CrossRef] PMID: 27854364.

Parisse, P., Rago, I., Ulloa Severino, L., Perissinotto, F., Ambrosetti, E., Paoletti, P., Ricci, M., Beltrami, A. P., Cesselli, D., & Casalis, L. (2017). Atomic force microscopy analysis of extracellular vesicles. *European Biophysical Journal*, *46*, 813–820.[CrossRef] PMID: 28866771.

Park, E. J., Prajuabjinda, O., Soe, Z. Y., Darkwah, S., Appiah, M. G., Kawamoto, E., Momose, F., Shiku, H., & Shimaoka, M. (2019). Exosomal regulation of lymphocyte homing to the gut. *Blood Advances*, *3*, 1–11.[CrossRef].

Pham, T. C., Jayasinghe, M. K., Pham, T. T., Yang, Y., Wei, L., Usman, W. M., Chen, H., Pirisinu, M., Gong, J., Kim, S., Peng, B., Wang, W., Chan, C., Ma, V., Nguyen, N. T. H., Kappei, D., Nguyen, X. - H., Cho, W. C., Shi, J., & Le, M. T. N. (2021). Covalent conjugation of extracellular vesicles with peptides and nanobodies for targeted therapeutic delivery. *Journal of Extracellular Vesicles*, *10*, e12057.[CrossRef] PMID: 33643546.

Phang, J. M., Harrop, S. J., Duff, A. P., Sokolova, A. V., Crossett, B., Walsh, J. C., Beckham, S. A., Nguyen, C. D., Davies, R. B., Glökner, C., Bromley, E. H. C., Wilk, K. E., & Curmi, P. M. G. (2016). Structural characterization suggests models for monomeric and dimeric forms of full-length ezrin. *Biochemical Journal*, *473*, 2763–2782.[CrossRef] PMID: 27364155.

Plaxco, K. W., & Gross, M. (2009). Protein complexes: The evolution of symmetry. *Current Biology*, *19*, R25–R26.[CrossRef].

R Development Core Team, R. (2011). *R: A Language and Environment for Statistical Computing*. R Foundation for Statistical Computing. Vienna, Austria.

Rai, A., Fang, H., Claridge, B., Simpson, R. J., & Greening, D. W. (2021). Proteomic dissection of large extracellular vesicle surfaceome unravels interactive surface platform. *Journal of Extracellular Vesicles*, 10, e12164.[CrossRef] PMID: 34817906.

Raimondo, F., Morosi, L., Chinello, C., Magni, F., & Pitto, M. (2011). Advances in membranous vesicle and exosome proteomics improving biological understanding and biomarker discovery. *Proteomics*, 11, 709–720.[CrossRef] PMID: 21241021.

Raposo, G., Nijman, H. W., Stoorvogel, W., Liejendekker, R., Harding, C. V., Melief, C. J., & Geuze, H. J. (1996). B lymphocytes secrete antigen-presenting vesicles. *Journal of Experimental Medicine*, 183, 1161–1172.[CrossRef] PMID: 8642258.

Raposo, G., & Stoorvogel, W. (2013). Extracellular vesicles: Exosomes, microvesicles, and friends. *Journal of Cell Biology*, 200, 373–383.[CrossRef] PMID: 23420871.

Roesengarth, A., & Luecke, H. (2004). Annexin A2: Does it induce membrane aggregation by a new multimeric state of the protein. *Annexins*, 1, 129.

Rontogianni, S., Synadaki, E., Li, B., Liefaard, M. C., Lips, E. H., Wesseling, J., Wu, W., & Altelaar, M. (2019). Proteomic profiling of extracellular vesicles allows for human breast cancer subtyping. *Communications Biology*, 2, 325.[CrossRef] PMID: 31508500.

Royo, F., Gil-Carton, D., Gonzalez, E., Mleczko, J., Palomo, L., Perez-Cormenzana, M., Mayo, R., Alonso, C., & Falcon-Perez, J. M. (2019). Differences in the metabolite composition and mechanical properties of extracellular vesicles secreted by hepatic cellular models. *Journal of Extracellular Vesicles*, 8, 1575678.[CrossRef] PMID: 30788084.

Sievers, F., Wilm, A., Dineen, D., Gibson, T. J., Karplus, K., Li, W., Lopez, R., Mcwilliam, H., Remmert, M., Söding, J., Thompson, J. D., & Higgins, D. G. (2011). Fast, scalable generation of high-quality protein multiple sequence alignments using Clustal Omega. *Molecular Systems Biology*, 7, 539.[CrossRef] PMID: 21988835.

Sinnott, M., Malhotra, S., Madhusudhan, M. S., Thalassinos, K., & Topf, M. (2020). Combining information from crosslinks and monolinks in the modeling of protein structures. *Structure (London, England)*, 28, 1061–1070.e3.[CrossRef].

Synowsky, S. A., Shirran, S. L., Cooke, F. G. M., Antoniou, A. N., Botting, C. H., & Powis, S. J. (2017). The major histocompatibility complex class I immunopeptidome of extracellular vesicles. *Journal of Biological Chemistry*, 292, 17084–17092.[CrossRef] PMID: 28860189.

Théry, C., Witwer, K. W., Aikawa, E., Alcaraz, M. J., Anderson, J. D., Andriantsitohaina, R., Antoniou, A., Arab, T., Archer, F., Atkin-Smith, G. K., Ayre, D. C., Bach, J. - M., Bachurski, D., Baharvand, H., Balaj, L., Baldacchino, S., Bauer, N. N., Baxter, A. A., Bebawy, M., …, Zuba-Surma, E. K. (2018). Minimal information for studies of extracellular vesicles 2018 (MISEV2018): a position statement of the International Society for Extracellular Vesicles and update of the MISEV2014 guidelines. *Journal of Extracellular Vesicles*, 7, 1535750.[CrossRef] PMID: 30637094.

Thind, A., & Wilson, C. (2016). Exosomal miRNAs as cancer biomarkers and therapeutic targets. *Journal of Extracellular Vesicles*, 5, 31292. [CrossRef] PMID:27440105.

Tian, F., Zhang, S., Liu, C., Han, Z., Liu, Y., Deng, J., Li, Y., Wu, X., Cai, L., Qin, L., Chen, Q., Yuan, Y., Liu, Y., Cong, Y., Ding, B., Jiang, Z., & Sun, J. (2021). Protein analysis of extracellular vesicles to monitor and predict therapeutic response in metastatic breast cancer. *Nature Communications*, 12, 1–13.[CrossRef] PMID: 33397941.

Tyanova, S., Temu, T., & Cox, J. (2016). The MaxQuant computational platform for mass spectrometry-based shotgun proteomics. *Nature Protocols*, 11, 2301–2319.[CrossRef] PMID: 27809316.

Vader, P., Mol, E. A., Pasterkamp, G., & Schiffelers, R. M. (2016). Extracellular vesicles for drug delivery. *Advanced Drug Delivery Reviews*, 106, 148–156.[CrossRef] PMID: 26928656.

Vangone, A., Spinelli, R., Scarano, V., Cavallo, L., & Oliva, R. (2011). COCOMAPS: A web application to analyze and visualize contacts at the interface of biomolecular complexes. *Bioinformatics*, 27, 2915–2916.[CrossRef] PMID: 21873642.

Van Zundert, G. C. P., & Bonvin, A. M. J. J. (2015). DisVis: Quantifying and visualizing accessible interaction space of distance-restrained biomolecular complexes. *Bioinformatics*, 31, 3222–3224.[CrossRef] PMID: 26026169.

Van Zundert, G. C. P., Rodrigues, J. P. G. L. M., Trellet, M., Schmitz, C., Kastritis, P. L., Karaca, E., Melquiond, A. S. J., Van Dijk, M., De Vries, S. J., & Bonvin, A. M. J. J. (2016). The HADDOCK2.2 web server: User-friendly integrative modeling of biomolecular complexes. *Journal of Molecular Biology*, 428, 720–725.[CrossRef] PMID: 26410586.

Van Zundert, G. C. P., Trellet, M., Schaarschmidt, J., Kurkcuoglu, Z., David, M., Verlato, M., Rosato, A., & Bonvin, A. M. J. J. (2017). The DisVis and PowerFit web servers: Explorative and integrative modeling of biomolecular complexes. *Journal of Molecular Biology*, 429, 399–407.[CrossRef] PMID: 27939290.

Vizcaíno, J. A., Csordas, A., Del-Toro, N., Dianes, J. A., Griss, J., Lavidas, I., Mayer, G., Perez-Riverol, Y., Reisinger, F., Ternent, T., Xu, Q. - W., Wang, R., & Hermjakob, H. (2016). 2016 update of the PRIDE database and its related tools. *Nucleic Acids Research*, 44, D447–D456.[CrossRef].

Waisman, D. M. (1995). Annexin II tetramer: Structure and function. *Molecular and Cellular Biochemistry*, 149, 301–322.[CrossRef] PMID: 8569746.

Wang, X., Shen, H., Zhangyuan, G., Huang, R., Zhang, W., He, Q., Jin, K., Zhuo, H., Zhang, Z., Wang, J., Sun, B., & Lu, X. (2018). 14-3-3ζ delivered by hepatocellular carcinoma-derived exosomes impaired anti-tumor function of tumor-infiltrating T lymphocytes. *Cell Death & Disease*, 9, 1–14.

Waterhouse, A., Bertoni, M., Bienert, S., Studer, G., Tauriello, G., Gumienny, R., Heer, F. T., De Beer, T. A. P., Rempfer, C., Bordoli, L., Lepore, R., & Schwede, T. (2018). SWISS-MODEL: Homology modelling of protein structures and complexes. *Nucleic Acids Research*, 46, W296–W303.[CrossRef].

Williams, C., Royo, F., Aizpurua-Olaizola, O., Pazos, R., Boons, G. - J., Reichardt, N. - C., & Falcon-Perez, J. M. (2018). Glycosylation of extracellular vesicles: Current knowledge, tools and clinical perspectives. *Journal of Extracellular Vesicles*, 7, 1442985.[CrossRef] PMID: 29535851.

Yang, X. H., Flores, L. M., Li, Q., Zhou, P., Xu, F., Krop, I. E., & Hemler, M. E. (2010). Disruption of laminin-integrin-CD151-focal adhesion kinase axis sensitizes breast cancer cells to ErbB2 antagonists. *Cancer Research*, 70, 2256–2263.[CrossRef] PMID: 20197472.

Zeev-Ben-Mordehai, T., Vasishtan, D., Siebert, C. A., Whittle, C., & Grünewald, K. (2014). Extracellular vesicles: A platform for the structure determination of membrane proteins by Cryo-EM. *Structure (London, England)*, 22, 1687–1692.

Zhang, D. X., Vu, L. T., Ismail, N. N., Le, M. T. N., & Grimson, A. (2021). Landscape of extracellular vesicles in the tumour microenvironment: Interactions with stromal cells and with non-cell components, and impacts on metabolic reprogramming, horizontal transfer of neoplastic traits, and the emergence of therapeutic resistance. *Seminars in Cancer Biology*, 74, 24–44.[CrossRef] PMID: 33545339.

Zhang, G., Huang, X., Xiu, H., Sun, Y., Chen, J., Cheng, G., Song, Z., Peng, Y., Shen, Y., Wang, J., & Cai, Z. (2020). Extracellular vesicles: Natural liver-accumulating drug delivery vehicles for the treatment of liver diseases. *Journal of Extracellular Vesicles*, 10, e12030.[CrossRef] PMID: 33335695.

Zhang, H., Freitas, D., Kim, H. S., Fabijanic, K., Li, Z., Chen, H., Mark, M. T., Molina, H., Martin, A. B., Bojmar, L., Fang, J., Rampersaud, S., Hoshino, A., Matei, I., Kenific, C. M., Nakajima, M., Mutvei, A. P., Sansone, P., Buehring, W., …, Lyden, D. (2018). Identification of distinct nanoparticles and subsets of extracellular vesicles by asymmetric flow field-flow fractionation. *Nature Cell Biology*, 20, 332–343.[CrossRef] PMID: 29459780.

Zhou, E., Li, Y., Wu, F., Guo, M., Xu, J., Wang, S., Tan, Q., Ma, P., Song, S., & Jin, Y. (2021). Circulating extracellular vesicles are effective biomarkers for predicting response to cancer therapy. *EBioMedicine*, 67, 103365.[CrossRef] PMID: 33971402.

Zhu, J., Cai, T., Zhou, J., Du, W., Zeng, Y., Liu, T., Fu, Y., Li, Y., Qian, Q., Yang, X. H., Li, Q., Huang, J. A., & Liu, Z. (2021). CD151 drives cancer progression depending on integrin $\alpha3\beta1$ through EGFR signaling in non-small cell lung cancer. *Journal of Experimental & Clinical Cancer Research*, *40*, 192.

Zipkin, M. (2020). Big pharma buys into exosomes for drug delivery. *Nature Biotechnology*, *38*, 1226–1228.[CrossRef] PMID: 33144725.

SUPPORTING INFORMATION

Additional supporting information can be found online in the Supporting Information section at the end of this article.

How to cite this article: Bauzá-Martinez, J., Armony, G., Pronker, M. F., & Wu, W. (2022). Characterization of protein complexes in extracellular vesicles by intact extracellular vesicle crosslinking mass spectrometry (iEVXL). *Journal of Extracellular Vesicles*, *11*, e12245. https://doi.org/10.1002/jev2.12245